



OPEN

Serine 937 phosphorylation enhances KCC2 activity and strengthens synaptic inhibition

Tamara Radulovic^{1,4}, Ezhilarasan Rajaram², Lena Ebbers³, Sara Pagella², Michael Winklhofer^{4,5}, Conny Kopp-Scheinflug², Hans Gerd Nothwang^{3,4,6}, Ivan Milenkovic^{1,4} & Anna-Maria Hartmann^{3,4,6} 

The potassium chloride cotransporter KCC2 is crucial for Cl⁻ extrusion from mature neurons and thus key to hyperpolarizing inhibition. Auditory brainstem circuits contain well-understood inhibitory projections and provide a potent model to study the regulation of synaptic inhibition. Two peculiarities of the auditory brainstem are (i) posttranslational activation of KCC2 during development and (ii) extremely negative reversal potentials in specific circuits. To investigate the role of the potent phospho-site serine 937 therein, we generated a KCC2 Thr^{934Ala}/Ser^{937Asp} double mutation, in which Ser⁹³⁷ is replaced by aspartate mimicking the phosphorylated state, and the neighbouring Thr⁹³⁴ arrested in the dephosphorylated state. This double mutant showed a twofold increased transport activity in HEK293 cells, raising the hypothesis that auditory brainstem neurons show lower [Cl⁻]_i and increased glycinergic inhibition. This was tested in a mouse model carrying the same KCC2 Thr^{934Ala}/Ser^{937Asp} mutation by the use of the CRISPR/Cas9 technology. Homozygous KCC2 Thr^{934Ala}/Ser^{937Asp} mice showed an earlier developmental onset of hyperpolarisation in the auditory brainstem. Mature neurons displayed stronger glycinergic inhibition due to hyperpolarized E_{Cl⁻}. These data demonstrate that phospho-regulation of KCC2 Ser⁹³⁷ is a potent way to interfere with the excitation-inhibition balance in neural circuits.

Proper brain function relies on a fine tuned balance between excitation and inhibition^{1,2}. Excitatory synaptic transmission is mainly mediated through glutamatergic synapses and inhibitory synaptic transmission through GABAergic and glycinergic signalling². Binding of GABA (gamma aminobutyric acid) and glycine to ionotropic GABA_A and glycine receptors, respectively³, results in Cl⁻ influx into mature neurons leading to hyperpolarizing inhibitory postsynaptic potentials (IPSPs). In contrast, in immature neurons GABA and glycine cause a depolarisation of the membrane due to Cl⁻ efflux driven by high [Cl⁻]_i⁴⁻⁹. Depolarisation in immature neurons facilitates opening of voltage-gated Ca²⁺ channels thereby evoking local Ca²⁺ transients¹⁰⁻¹⁶. Ca²⁺ in turn activates intracellular signalling cascades, which are important to establish and stabilize synaptic connections^{12,15,17}. The developmental shift from depolarisation to hyperpolarisation (D/H shift) is conserved throughout the nervous system (e.g. brainstem, cortex, hippocampus, hypothalamus, and spinal cord)^{4,6,8,12,13,18-20} and occurs during early postnatal life in most rodents^{21,22}.

The key players regulating the D/H shift are NKCC1 (sodium potassium chloride cotransporter 1) and KCC2 (potassium chloride cotransporter 2)²³⁻²⁶. Both membrane transporters are secondary active mediating the Cl⁻ coupled transport of K⁺ and/or Na⁺^{27,28}. In immature neurons, NKCC1 is the predominant transporter mediating Cl⁻ uptake and intracellular accumulation²⁹⁻³². In mature neurons, KCC2 is the central Cl⁻ extruder that lowers [Cl⁻]_i and thus enables fast hyperpolarizing postsynaptic inhibition^{33,34}. The physiological relevance of NKCC1 and KCC2 is underlined by the severe phenotypes of knock-out mice models. Mice with disruption of the gene *Slc12a5* encoding both splice variants of KCC2 (KCC2a and KCC2b) die shortly after birth due to severe motor

¹Division of Physiology School of Medicine and Health Sciences, Carl Von Ossietzky University Oldenburg, 26111 Oldenburg, Germany. ²Division of Neurobiology, Faculty of Biology, Ludwig-Maximilians-University Munich, 82152 Planegg-Martinsried, Germany. ³Division of Neurogenetics, School of Medicine and Health Sciences, Carl Von Ossietzky University Oldenburg, 26111 Oldenburg, Germany. ⁴Research Center Neurosensory Science, Carl Von Ossietzky University Oldenburg, 26111 Oldenburg, Germany. ⁵Institute for Biology and Environmental Sciences IBU, Carl Von Ossietzky University of Oldenburg, 26111 Oldenburg, Germany. ⁶Center of Excellence Hearing4all, Carl Von Ossietzky University Oldenburg, 26111 Oldenburg, Germany. ✉email: anna.maria.hartmann@uol.de

deficits that compromise respiration^{35,36}. Mice with disruption of the gene *Slc12a2* encoding NKCC1 are viable, but suffer from deafness, increased pain perception, and male infertility^{31,37–39}.

In most brain areas including cortex, hippocampus and the cerebellum, the D/H shift is caused by a decrease in NKCC1 and an increase in KCC2 expression during development^{31,33,40–46}. Interestingly, auditory brainstem neurons perinatally express KCC2 at high levels in the plasma membrane, but in a transport-inactive form^{47–49}. Here, the developmental increase in KCC2 transport activity correlates with an increase in the oligomer/monomer ratio⁴⁹ and a switch from membrane rafts to non-membrane rafts⁵⁰. In addition, phospho-regulation may play an essential role in the developmental activation of KCC2^{51,52}, but detailed knowledge of the multiple phosphorylation sites is lacking.

In the mature auditory brainstem, synaptic inhibition is key in various computational tasks during neural signal processing. This is reflected by well-defined inhibitory projections and circuit-specific hyperpolarizing glycine reversal potentials (E_{Gly}). The superior paraolivary nucleus (SPN) is involved in encoding sound offsets⁵³ and displays an exceptionally negative $E_{Gly} = -90.6$ mV, compared to other auditory nuclei, such as the auditory lateral superior olive (LSO) ($E_{Gly} = -68.6$ mV) and the medial superior olive (MSO) ($E_{Gly} = -75.8$ mV) in mice⁵⁴.

Differential phosphorylation of KCC2 could be one mechanism underlying different E_{Gly} in neuronal subtypes. KCC2 harbours several phosphorylation sites that are present at the N-terminus and C-terminus and have been shown to impact its transport activity^{28,55–57}. Interestingly, both dephosphorylation of Thr⁶ in KCC2a, Thr⁹⁰⁶, Thr¹⁰⁰⁷, Thr¹⁰⁰⁹, and Tyr¹⁰⁸⁷ and phosphorylation of Ser⁹³², Thr⁹³⁴, Ser⁹³⁷, and Ser⁹⁴⁰ enhances KCC2 activity^{52,57–69}. The latter phospho-sites are all encoded by exon 22, which is only present in KCC2 and non-therian KCC4 (Fig. 1)^{65,66,69–71}. These complex phosphorylation and dephosphorylation combinations provide KCC2 with a rich-regulatory tool-box to achieve graded activity and the integration of different signalling pathways^{60,66}.

Here, we used CRISPR/Cas9 gene editing to generate transgenic mice with a Thr^{934Ala}/Ser^{937Asp} double mutation in KCC2 to probe for a functional link between KCC2 phosphorylation and its transport activity.

Results

Phosphorylation of Ser⁹³⁷ in the KCC2a Thr^{934Ala}/Ser^{937Asp} double mutant enhances KCC2 transport activity

Serine 937 represents an experimentally proven phosphorylation site^{58,65}. It might sometimes be flanked by phosphorylation of threonine 934⁵⁸. A previous analysis demonstrated that single mutation of threonine 934 or serine 937 into aspartate (mimicking the phosphorylated state) increases KCC2 activity twofold, whereas mutation of either of the two residues into alanine (mimicking the dephosphorylated state) does not impair KCC2 activity⁶⁵. Here, we generated a KCC2 Thr^{934Ala}/Ser^{937Asp} double mutant that traps Ser⁹³⁷ in the phosphorylated state (Thr^{934Ala}) and the nearby Thr⁹³⁴ in the dephosphorylated state (Ser^{937Asp}). Importantly, the latter mutation Thr^{934Ala} alone does not alter KCC2 activity⁶⁵. This Thr^{934Ala}/Ser^{937Asp} mutant enabled us to specifically investigate the effect of Ser⁹³⁷ phosphorylation on the activity. The double mutation also prevents a possible confounding action of phosphatases and kinases on threonine 934, which might render interpretation of the results difficult. Immunocytochemical analyses of the transiently transfected KCC2 constructs in HEK293 cells revealed similar transfection rates between KCC2a wild-type (KCC2a^{WT}) and KCC2a Thr^{934Ala}/Ser^{937Asp} (Fig. 2B). To analyse the transport activity, we used the well-established Tl⁺ flux measurement method^{65,66,72,73}. HEK293 cells transfected with KCC2a^{WT} showed higher transport activity than in mock transfected cells (100 ± 9.05% vs. 28.92 ± 14.23%; $p = 1.93 \times 10^{-10}$) (Fig. 2A, Table 1). In comparison, the KCC2a Thr^{934Ala}/Ser^{937Asp} double mutant showed twofold higher transport activity compared to KCC2a^{WT} (199 ± 44.96%; $p = 0.001$) (Fig. 2A, Table 1). These data reveal that phosphorylation of Ser⁹³⁷ in Thr^{934Ala}/Ser^{937Asp} double mutant enhances the activity.

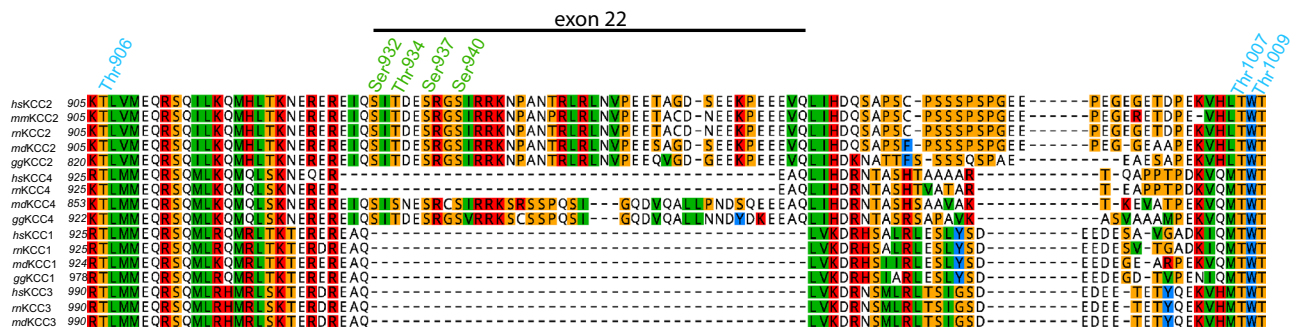


Figure 1. Evolutionary conservation of phosphorylation site in vertebrate KCC isoforms. Multialignment of a C-terminal part of vertebrate KCCs were generated using ClustalW in Genious. Amino acid residues encoded by exon 22 are marked by a black bar. Exon 22 is only present in all vertebrate KCC2 and non-therian KCC4 isoforms. Phosphorylation sites that enhance KCC2 activity upon dephosphorylation are marked with blue asterisks. These phosphorylation sites are Thr⁹⁰⁶, Thr¹⁰⁰⁷ and Thr¹⁰⁰⁹. They are highly conserved among all vertebrate KCC isoforms. Phosphorylation sites that are marked with green asterisks enhance KCC2 activity upon phosphorylation. These sites are Ser⁹³², Thr⁹³⁴, Ser⁹³⁷, and Ser⁹⁴⁰. They are only present in KCC isoforms encoded by exon 22. *hs* (*Homo sapiens*), *mm* (*mus musculus*), *rn* (*Rattus norvegicus*), *md* (*Monodelphis domestica*), *gg* (*Gallus gallus*).

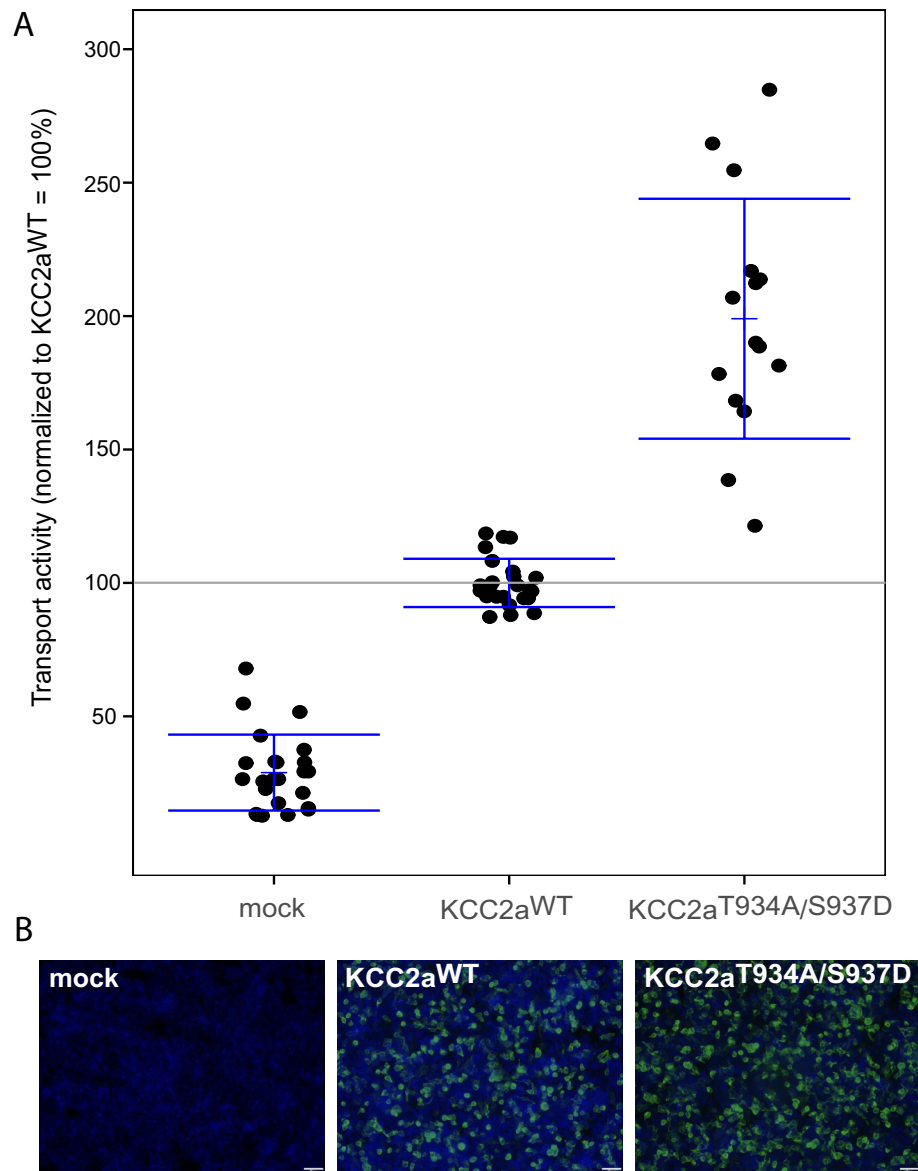


Figure 2. The KCC2 Thr^{934Ala}/Ser^{937Asp} double mutant enhances KCC2 activity. HEK293 cells were transiently transfected with KCC2a^{WT} or KCC2a Thr^{934Ala}/Ser^{937Asp}. **(A)** Tl⁺ flux measurement was performed to determine the KCC2 transport activity. KCC2a^{WT} displayed a significant higher transport activity ($100 \pm 1.8\%$, $p = 1.93 \times 10^{-10}$) than mock transfected cells ($24 \pm 2.9\%$). The KCC2a Thr^{934Ala}/Ser^{937Asp} double mutant ($199 \pm 11.6\%$) significantly enhances KCC2 transport activity ($p = 0.001$). The graph represents the data of at least five independent measurements including three technical replicates per independent measurement, normalized to KCC2a^{WT}. Depicted are mean values \pm SE. **(B)** Immunocytochemistry was used to monitor the transfection rate of KCC2 (green) and cell staining by DAPI (blue). The scale bar is 200 μ m.

	Average and SE	Significance in comparison to KCC2 ^{wt}	Significance in comparison to mock
mock	$24\% \pm 2.9\%$	***	–
KCC2 ^{wt}	$100\% \pm 1.8\%$	–	***
Thr ^{934Ala} /Ser ^{937Asp}	$199\% \pm 11.6\%$	***	***

Table 1. Transport activity of KCC2a constructs. *** $p < 0.001$.

Homozygous $KCC2$ Thr^{934Ala}/Ser^{937Asp} mice show no obvious phenotypic changes

To analyse the *in vivo* impact of Ser⁹³⁷ phosphorylation, we generated a $KCC2$ Thr^{934Ala}/Ser^{937Asp} mice via CRISPR/Cas9 located in exon 22 (Fig. 3A). The two mutations were verified by genotyping and DNA sequencing. Heterozygous and homozygous $KCC2$ Thr^{934Ala}/Ser^{937Asp} mice, which we here name $KCC2^{+/AD}$ (heterozygous) and $KCC2^{AD/AD}$ (homozygous) are viable, fertile, showing no abnormalities in the nutritional state, posture, motor skills and coat. The genotypes of the littermates show the expected Mendelian inheritance of the two alleles (χ^2 -test 1:2:1; Table 2). Compared to $KCC2^{+/+}$ littermates, heterozygous $KCC2^{+/AD}$ and homozygous $KCC2^{AD/AD}$ mice show no differences in weight gain from P0 to P16 (Fig. 3B, Table 3, p -value = 0.76, see ANOVA output in Table 4). As usual, male mice become slightly heavier than females (p -value = 0.025, see Table 4), without a genotype-specific effect (p -value = 0.65). Thus, heterozygous $KCC2^{+/AD}$ and homozygous $KCC2^{AD/AD}$ mice show no obvious phenotypic changes.

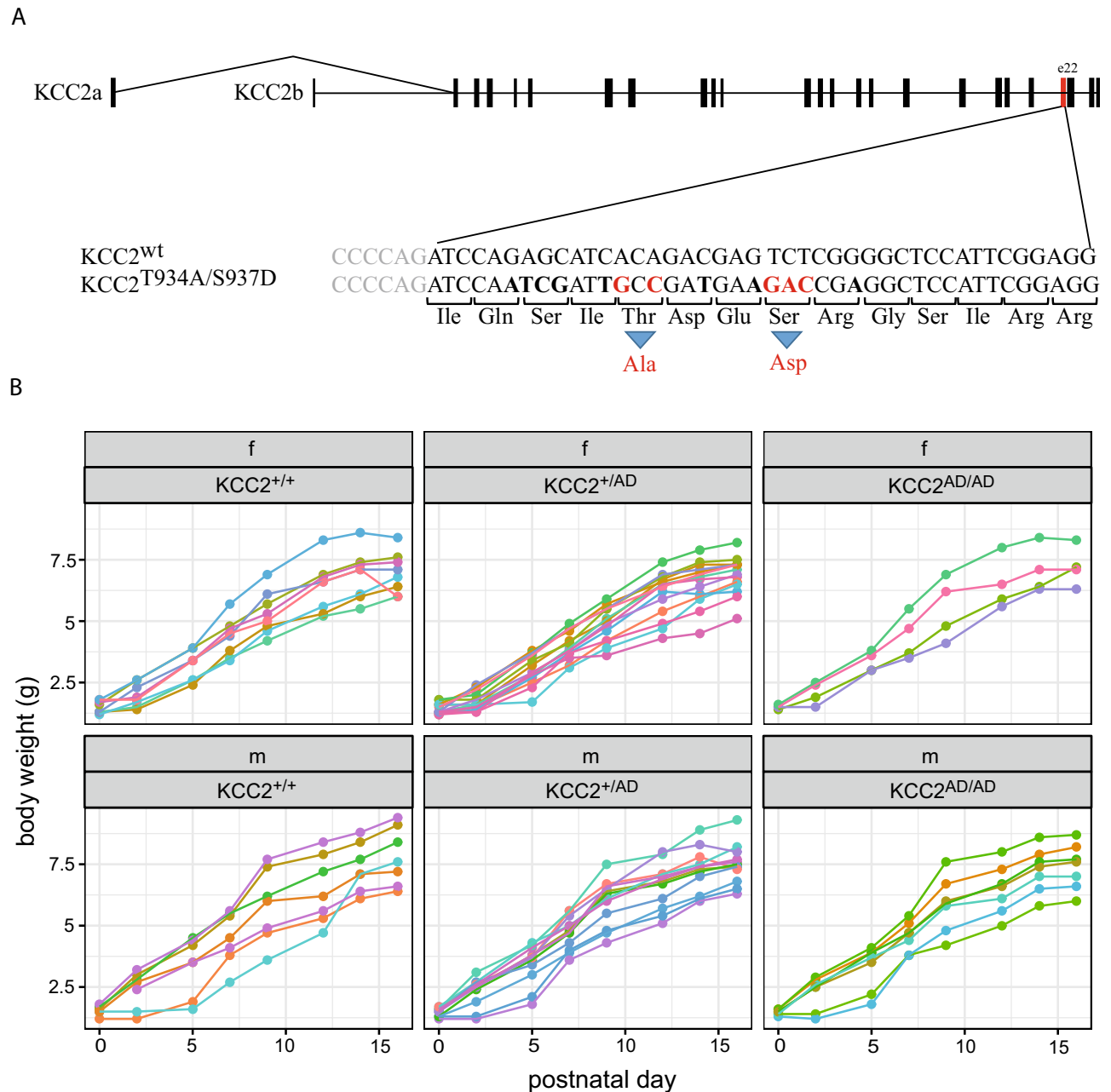


Figure 3. Characterization of transgenic $KCC2$ Thr^{934Ala}/Ser^{937Asp} mice. (A) The transgenic $KCC2$ Thr^{934Ala}/Ser^{937Asp} mouse line was generated with CRISPR/Cas. Here, Thr⁹³⁴ was mutated to alanine and Ser⁹³⁷ was mutated to aspartate. Both phosphorylation sites are located in exon 22. (B) Compared to $KCC2^{+/+}$ littermates ($n = 15$), heterozygous ($KCC2^{+/AD}$, $n = 26$) and homozygous ($KCC2^{AD/AD}$, $n = 12$) mice show no differences in weight gain from P0 to P16 (Tables 3 and 4).

KCC2	Number of littermates		Chi ²	df	p-value
	Observed	Expected			
+/+	15	13.25	0.36	2	0.83
+AD	26	26.5			
AD/AD	12	13.25			

Table 2. Chi² test of the birth rate according to Mendel. +/+ : Homozygous KCC2^{WT} mice, +AD: heterozygous Thr^{934Ala}/Ser^{937Asp} mice, AD/AD: homozygous Thr^{934Ala}/Ser^{937Asp} mice.

KCC2	Sex	n	P0	P2	P5	P7	P9	P12	P14	P16
+/+	Female	8	1.50 g ± 0.25 g	1.98 g ± 0.47 g	3.20 g ± 0.59 g	4.35 g ± 0.77 g	5.33 g ± 0.88 g	6.41 g ± 1.03 g	6.89 g ± 0.98 g	6.96 g ± 0.83 g
	Male	7	1.55 g ± 0.21 g	2.40 g ± 0.76 g	3.37 g ± 1.18 g	4.51 g ± 1.07 g	5.79 g ± 1.48 g	6.47 g ± 1.39 g	7.37 g ± 0.99 g	7.81 g ± 1.18 g
+AD	Female	14	1.43 g ± 0.22 g	1.74 g ± 0.36 g	3.00 g ± 0.61 g	3.99 g ± 0.57 g	4.89 g ± 0.71 g	6.09 g ± 0.92 g	6.53 g ± 0.89 g	6.86 g ± 0.76 g
	Male	12	1.48 g ± 0.17 g	2.33 g ± 0.57 g	3.46 g ± 0.79 g	4.72 g ± 0.66 g	5.95 g ± 0.95 g	6.65 g ± 0.91 g	7.26 g ± 0.87 g	7.50 g ± 0.80 g
AD/AD	Female	5	1.48 g ± 0.08 g	2.10 g ± 0.41 g	3.32 g ± 0.36 g	4.30 g ± 0.81 g	5.48 g ± 1.11 g	6.34 g ± 0.99 g	6.96 g ± 0.86 g	7.12 g ± 0.75 g
	Male	7	1.47 g ± 0.11 g	2.27 g ± 0.68 g	3.30 g ± 0.91 g	4.56 g ± 0.61 g	5.86 g ± 1.13 g	6.47 g ± 1.01 g	7.26 g ± 0.92 g	7.40 g ± 0.93 g

Table 3. Weight of KCC2 mice. +/+ : Homozygous KCC2^{WT} mice, +AD: heterozygous Thr^{934Ala}/Ser^{937Asp} mice, AD/AD: homozygous Thr^{934Ala}/Ser^{937Asp} mice.

Factor	Df	Sum Sq	Mean Sq	F value	p-value
Sex	1	21.28	21.283	5.351	0.025
Genotype	2	2.19	1.094	0.275	0.76
Sex:genotype	2	3.40	1.701	0.428	0.65
(Residuals)	46	182.97	3.978		

Table 4. Two-way repeated measurement ANOVA of weight of KCC2 mice. Df: Degrees of freedom, Sum Sq: Sum squares, Mean Sq: mean squares, F: F (mean Sq(factor)/MeanSq (res), Df(factor), Df(res)).

Next, we performed morphometric measurements in the auditory brainstem. Quantitative analysis of Nissl-stained sections of the brainstem revealed no significant changes in volume of major auditory nuclei. Both the dorsal (DCN) and ventral (VCN) parts of the cochlear nucleus complex (DCN: KCC2^{+/+}: 0.192 ± 0.022 mm³, KCC2^{AD/AD}: 0.171 ± 0.025 mm³, $p = 0.334$; VCN: KCC2^{+/+}: 0.249 ± 0.037 mm³, KCC2^{AD/AD}: 0.223 ± 0.014 mm³, $p = 0.315$; Fig. 4A,B) were not affected. Nuclei of the superior olivary complex showed also no morphological differences. All three examined nuclei, the lateral superior olive (LSO), the superior paraolivary nucleus (SPN), and the medial nucleus of the trapezoid body (MNTB) showed no change in volume (LSO: KCC2^{+/+}: 0.054 ± 0.003 mm³, KCC2^{AD/AD}: 0.050 ± 0.003 mm³, $p = 0.208$; SPN: KCC2^{+/+}: 0.027 ± 0.005 mm³, KCC2^{AD/AD}: 0.023 ± 0.001 mm³, $p = 0.239$; MNTB: KCC2^{+/+}: 0.034 ± 0.005 mm³, KCC2^{AD/AD}: 0.034 ± 0.001 mm³, $p = 0.315$; Fig. 4A,C). Thus, the phosphorylation mimic of Ser⁹³⁷ does not affect gross morphology of the auditory brainstem, probably ruling out effects on cell migration or cell viability.

Earlier D/H shift in LSO neurons of homozygous KCC2 Thr^{934Ala}/Ser^{937Asp} mice

The action of glycine, the main inhibitory neurotransmitter in the brainstem, shows a D/H shift between P4 and P8 in LSO neurons^{8,20,47,74,75}. To access whether phosphorylation of KCC2 affects its transport activity, we performed gramicidin perforated patch clamp recordings in LSO neurons at the ages P3 and P5, as previously described^{76–78}. To this end, the reversal potential of glycine-evoked currents was determined while leaving the [Cl⁻]_i undisturbed through gramicidin-pores that are exclusively permeable to monovalent cations and small, uncharged molecules^{79,80}. Glycine was applied via puff-application (100 ms) at saturating concentration of 1 mM, while neurons were held at different membrane potentials. Synaptic stimulation can not be used to reliably estimate E_{Cl⁻} at this immature stage, due to ongoing development of inhibitory inputs^{20,81–83}. In control mice, we measured a depolarized E_{Cl⁻} at P3 compared to P5 (Fig. 5) and hypothesized in homozygous KCC2^{AD/AD} mice a more hyperpolarized E_{Cl⁻} with respect to controls. In the control data set containing cells from wild type (KCC2^{+/+}) littermates and C57Bl/6N animals, we recorded the average E_{Cl⁻} at P3 = -36.6 mV (n = 7) and at P5 = -63.8 mV (n = 5), in agreement with a developmental shift toward hyperpolarizing values (**, $p = 0.002$). In contrast, recordings in KCC2^{AD/AD} LSO neurons showed the average E_{Cl⁻} = -79.4 mV (n = 5) already at P3, with no further change at P5 (E_{Cl⁻} = -71 mV, n = 5, $p = 0.155$). These data demonstrate that the phospho-mimetic

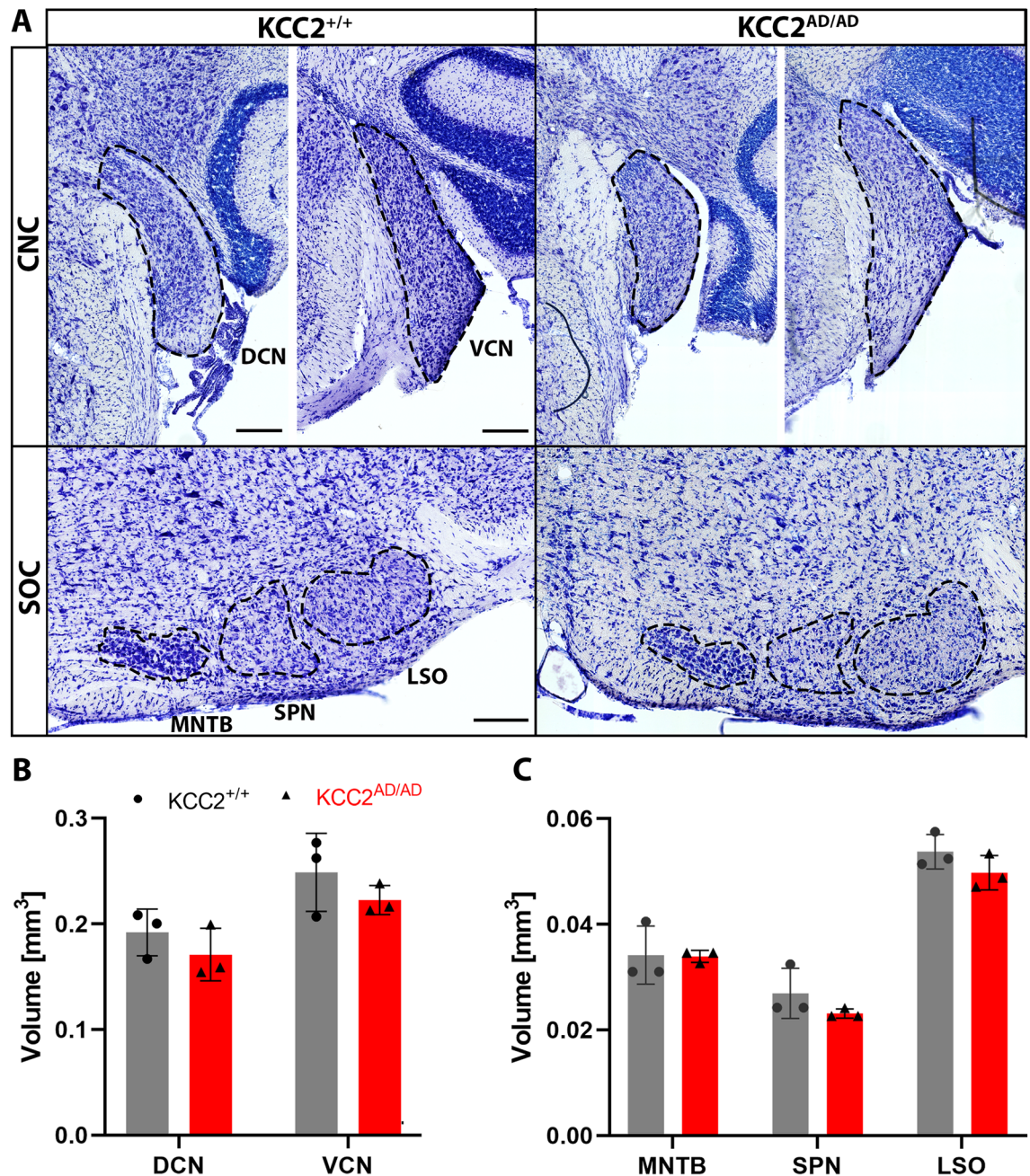


Figure 4. No morphological changes in the auditory brainstem of homozygous KCC2 Thr⁹³⁴Ala/Ser⁹³⁷Asp mice. (A) Representative images of Nissl-stained sections of the auditory brainstem nuclei of adult homozygous KCC2^{WT} (KCC2^{+/+}) and KCC2 Thr⁹³⁴Ala/Ser⁹³⁷Asp (KCC2^{AD/AD}) mice. Quantitative morphometric analyses revealed no differences in volume of the nuclei of the CNC (B) as well as of the SOC (C) between the two genotypes. Depicted are mean values \pm SD, N = 3 mice/genotype; scale bar = 200 μ m. CNC, cochlear nucleus complex; DCN, dorsal cochlear nucleus; LSO, lateral superior olive; MNTB, medial nucleus of the trapezoid body; SOC, superior olivary complex; SPN, superior paraolivary nucleus; VCN, ventral cochlear nucleus.

mutation of KCC2 at Ser⁹³⁷ causes an early D/H shift of E_{Cl}⁻ compared to the control (-79.4 mV vs. -36.6 mV at P3, ****p* < 0.001), suggesting an important role of this phospho-site in developmental regulation of KCC2.

Adult homozygous KCC2 Thr⁹³⁴Ala/Ser⁹³⁷Asp mice show more hyperpolarized IPSC-reversal potentials

Based on the increased Cl⁻ extrusion activity of KCC2 observed in HEK293 cells and immature neurons, we predicted more hyperpolarized reversal potentials for synaptically evoked inhibition (E_{IPSCs}) in mature LSO and SPN neurons. We tested this hypothesis by taking advantage of whole cell patch-clamp recordings that allowed to set high intracellular Cl⁻ concentrations of 34.5 mM in order to further challenge KCC2's Cl⁻ extrusion activity. Based on the Nernst equation, the compositions of pipette solution, the ACSEF, the junction potential correction

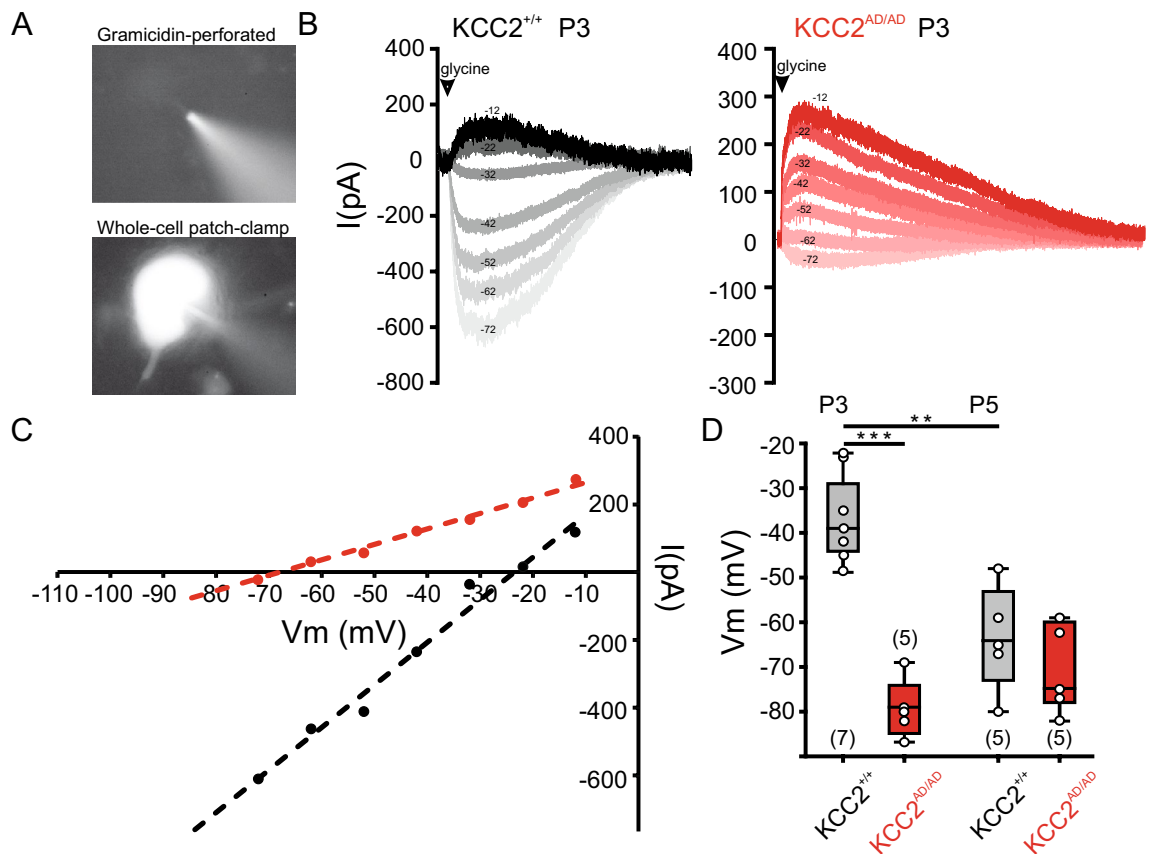


Figure 5. Earlier D/H shift in homozygote $KCC2\ Thr^{934Ala}/Ser^{937Asp}$ mice. Gramicidin perforated recording in LSO neurons. (A) (*up*) image of gramicidin perforated recording, visible patch pipette loaded with Atto 488; (*below*) whole-cell recording configuration with Atto488 inside the cell following patch rupture. (B) Representative traces from recordings made in control ($KCC2^{+/+}$) and homozygous $KCC2\ Thr^{934Ala}/Ser^{937Asp}$ ($KCC2^{AD/AD}$) group at P3 showing current traces in response to glycine application at different holding potentials. (C) Representative plot of peak current amplitudes at different voltages for both groups at P3 (black control, red $KCC2^{AD/AD}$). Line intersection with x-axis indicates the E_{Cl^-} . (D) Population data from control and $KCC2^{AD/AD}$ at P3 and P5 showing significantly hyperpolarized E_{Cl^-} at P3 in $KCC2^{AD/AD}$ compared to control. The control group shows a developmental change towards hyperpolarized values from P3 to P5.

and the assumption that glycinergic synaptic currents are mainly carried by Cl^- , the predicted E_{IPSC} was $-36\ mV$. However, electrical stimulation of the inhibitory fibre tracts leaving the MNTB, the major source of glycinergic inhibition in the superior olivary complex (Fig. 6A,B), reliably elicited pharmacologically isolated glycinergic IPSCs with E_{IPSCs} of at least $-70\ mV$ in wild type $KCC2^{+/+}$ and homozygous $KCC2^{AD/AD}$ mice. The driving force of the IPSCs, or else the strength of inhibition, is governed by the difference between the resting (in our case holding) potential and the reversal potential of the IPSC. IPSCs of homozygous $KCC2^{AD/AD}$ neurons reversed at more hyperpolarized membrane potentials compared to wild type neurons, suggesting a larger driving force for inhibition in homozygous $KCC2^{AD/AD}$ mice and thus increased KCC2 activity (Fig. 6C,D). These more hyperpolarizing IPSCs resulted in a leftward shift of the current–voltage relationship in both LSO and SPN neurons (Fig. 6E,F), which changed from $-72.0 \pm 2.6\ mV$ ($n = 11$) in LSO wild type neurons to $-80.6 \pm 2.7\ mV$ ($n = 12$) $KCC2^{AD/AD}$ neurons (two-tailed t -test: $p = 0.034$; Fig. 6G). A hyperpolarizing shift was also observed from $-82.0 \pm 2.1\ mV$ ($n = 19$) in wild type SPN neurons to $-92.8 \pm 1.4\ mV$ ($n = 13$) $KCC2^{AD/AD}$ neurons (two-tailed t -test: $p \leq 0.001$; Fig. 6G). Thus, the phospho-mimetic mutation at Ser^{937} affects not only the developmental shift in immature auditory neurons, but also increases the driving force for inhibition in mature neurons.

Discussion

We generated a transgenic $KCC2\ Thr^{934Ala}/Ser^{937Asp}$ mouse, in which serine 937 is replaced by aspartate mimicking the phosphorylated state and analysed its role in the auditory brainstem. This approach was motivated by the observation that the phospho-mimetic mutation of serine 937 is among the most effective ways to increase KCC2 activity in a heterologous expression system⁶⁵, and since the auditory brainstem shows peculiarities concerning synaptic inhibition, such as posttranslational activation of KCC2 to induce D/H shift^{47,49} and the most negative E_{Cl^-} observed so far in neurons⁵⁴.

A fundamental process during development of the nervous system is the shift from depolarizing to hyperpolarizing action of inhibitory neurotransmitters. This is often accompanied by an increase in the expression or increase in the activity of KCC2^{33,40–44,46}. In the auditory brainstem, especially in rat LSO neurons, the D/H shift

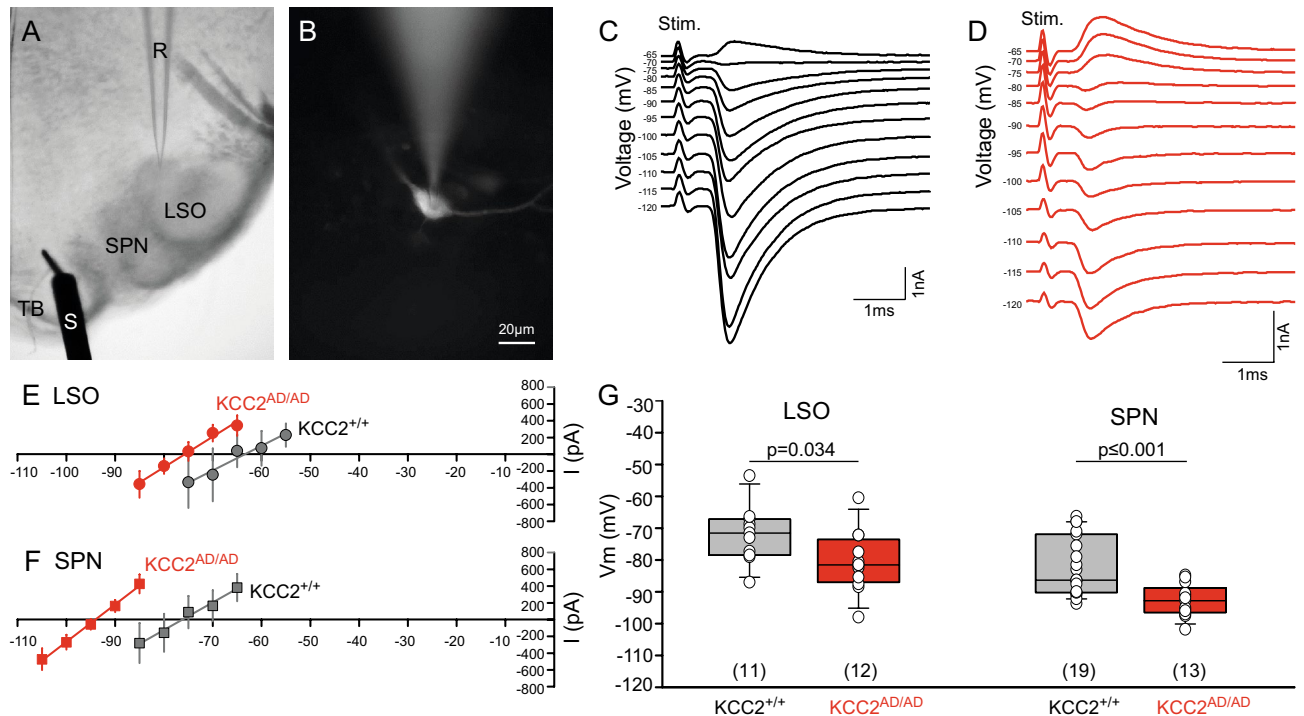


Figure 6. Hyperpolarized E_{Cl^-} in mature LSO and SPN neurons of homozygous KCC2 Thr^{934Ala}/Ser^{937Asp} mice. (A) Coronal slice at the level of the superior olive showing the bipolar stimulation electrode (left) in the MNTB and a patch pipette (right) in the LSO. (B) Low magnification image of an LSO neuron filled with dye via the patch pipette. (C), (D) Synaptically evoked IPSCs recorded in LSO neurons of wild type (KCC2^{+/+}) (C) and homozygous KCC2 Thr^{934Ala}/Ser^{937Asp} (KCC2^{AD/AD}) mice (D) over a range of holding potentials (–120 to –65 mV). (E), (F) The mean I/V relationship for the IPSCs in wild type neurons (black) and KCC2^{AD/AD} neurons (red) revealed a left shift towards more hyperpolarized IPSC reversal potentials (=line intersection with x-axis) in the LSO (E) and the SPN (F). (G) This difference in reversal potentials was significant for mature neurons in the LSO and SPN.

occurs during the first postnatal week^{8,20,74,75,84}. Here, KCC2 is perinatally expressed, but transport-inactive^{47,49}. This raises the question how KCC2 activation is achieved during development^{47,49}. Based on previous studies, three possible scenarios can be envisaged, which might be causally related: increase in the oligomer/monomer ratio⁴⁹, a shift from membrane rafts to non-membrane rafts⁵⁰, and phospho-regulation^{51,85}.

Here, we hypothesized that the potent phospho-site serine 937 plays an important role and, therefore, generated KCC2 Thr^{934Ala}/Ser^{937Asp} mice. These mice are viable and bred normally. They thus provide an excellent tool to explore in vivo the effect of phosphorylation on KCC2 activation and activity. By performing electrophysiological analyses in LSO neurons of acute brainstem slices, we showed that the developmental maturation of Cl⁻ dependent inhibition is shifted to earlier stages in homozygous KCC2 Thr^{934Ala}/Ser^{937Asp} mice. These results are consistent with in vitro analyses, as the KCC2 Thr^{934Ala}/Ser^{937Asp} double mutant leads to activation of KCC2 in HEK293 cells. Such enhanced KCC2 activity lowers the [Cl⁻]_i and increases the strength of glycinergic inhibition. Thus, phosphorylation of Ser⁹³⁷ is sufficient to induce KCC2 activity causing an earlier D/H shift in LSO neurons.

Similarly, (de)phosphorylation of Thr⁹⁰⁶/Thr¹⁰⁰⁷ or Ser⁹⁴⁰ induce the onset of hyperpolarisation during development^{86,87}. The decrease in phosphorylation of Thr⁹⁰⁶ and Thr¹⁰⁰⁷ increased KCC2 activity⁶⁰. In transgenic KCC2 Thr^{906Ala}/Thr^{1007Ala} mice, mimicking the dephosphorylated state of these two phospho-sites, an accelerated onset of hyperpolarisation in hippocampal neurons was observed, pointing to its importance for the D/H shift in this brain area⁸⁶. In contrast, heterozygous KCC2 Thr^{906Glu}/Thr^{1007Glu} mice, mimicking a phosphorylated state, showed a delayed D/H shift in CA3 pyramidal neurons and hippocampal slices⁸⁷. These mice showed increased ultra-sonic vocalization, seizure susceptibility and long-term abnormalities in social behaviour⁸⁷ in comparison to transgenic KCC2 Thr^{906Ala}/Thr^{1007Ala} mice. In the latter, the dephosphorylation-mimicking status limits the onset and severity of seizure⁶⁴. Ser⁹⁴⁰ is another phosphorylation site highly phosphorylated in cultured hippocampal neurons in the first postnatal week⁸⁶. This enhances the KCC2 activity in cultured hippocampal neurons^{69,86,88}. The importance of Ser⁹⁴⁰ phosphorylation is further corroborated by a delayed D/H shift in Ser^{940Ala} knock-in mice⁸⁶. These mice suffer from profound social interaction abnormalities like in autism spectrum disorders^{24,86}. Thus, phospho-regulation is a common mechanism to regulate KCC2 activity and to initiate the onset of hyperpolarisation. In view of its rich phospho-site tool box, it will be interesting to study in the future, whether individual phospho-sites have brain area-specific functions. The increasing number of site-specific KCC2 transgenic mice pave the way for such an analysis.

So far, it is unclear whether the stronger Cl⁻ extrusion in the transgenic KCC2^{AD/AD} mice has an implication for the auditory function. Presently, our gramicidin-perforated patch-clamp recordings revealed a conspicuous

early D/H shift in $KCC2^{AD/AD}$ mice (hyperpolarizing Cl^- gradient present at P3), suggesting early onset of $KCC2$ -mediated Cl^- extrusion. This result implies a shorter depolarizing phase of inhibitory inputs onto LSO neurons during postmitotic differentiation. In this phase of neuronal maturation, GABA/glycine triggered depolarisation increase $[Ca^{2+}]_i$, thus contributing to synaptic maturation during development of neuronal circuits⁹. In the early postnatal LSO, GABA/glycine synaptic inputs evoke depolarizing EPSPs which induce Ca^{2+} transients spreading to dendritic processes and even trigger action potentials^{8,15,20,89}. During the first postnatal week, such excitation likely facilitates NMDA-dependent developmental plasticity, thereby contributing to synaptic refinement of the MNTB-LSO projections⁹⁰. It remains to be investigated whether a shorter depolarizing phase, caused by early $KCC2$ activity onset, affects the development of excitatory and inhibitory synapses on LSO or SPN neurons.

The D/H shift in the auditory brainstem is staggered in time, occurring before postnatal day 1 (P1) in the SPN to about P12 (i.e. at hearing onset) in the MNTB (cochlear nucleus:^{48,76}; superior olivary complex:^{8,47,74,91}). While the mechanisms underlying cell-type-specific regulation remain to be elucidated, these differences point to the importance of precise Cl^- homeostasis regulation for maturation of the brainstem circuit.

Another peculiarity of the auditory brainstem is an extremely negative E_{Gly} specifically in mature SPN neurons⁵⁴. This is important for the precise offset firing after sound termination⁵³. The neuron-type-specific regulation of E_{Cl^-} in auditory brainstem neurons might be due to a different phosphorylation pattern of $KCC2$ that specifically attunes the strength of inhibition. Consistent with this notion, the phosphorylation status correlates with hyperpolarizing Cl^- gradient, as shown for E_{GABA} in adult hippocampal neurons of $Thr^{906Ala}/Thr^{1007Ala}$ transgenic mice⁶⁴. Our analyses of $KCC2^{AD/AD}$ mice demonstrate a more negative E_{IPSC} both in SPN and LSO neurons compared to $KCC2^{WT}$. However, the present data do not explain the E_{Cl^-} difference between SPN and LSO neurons, as the mutation caused a similar hyperpolarizing shift of about -10 mV in both nuclei. Therefore, it is tempting to presume additional regulatory mechanisms rendering E_{Gly} more negative in the SPN. In the future, phospho-proteomic studies or phospho-site specific immunohistochemistry will be helpful to investigate the different phosphorylation pattern of $KCC2$ in SPN and LSO neurons. What effect will the more negative reversal potential have in SPN neurons? Remarkably, SPN neurons show very stable, strongly hyperpolarized IPSC reversal potentials after the D/H shift has taken place, without further changes after hearing onset around P12⁹². This suggests that the crucial window for adjusting the strength of inhibition is indeed around the D/H shift. Behavioural effects are to be expected in difficult sound localization tasks as well as gap-detection or sound duration discrimination tasks. Indeed, a reduction of $KCC2$ activity results in reduced gap detection in a cellular paradigm⁵⁴. This loss of temporal resolution is present in ageing, hearing loss, and neurodegeneration⁵⁴. Our results suggest that phosphorylation of Ser^{937} enhances $KCC2$ activity resulting in more negative reversal potential in SPN neurons, which in turn might enhance gap detection. Therefore, pharmaceuticals that mediate a neuronal-targeted increase in phosphorylation of Ser^{937} may represent a novel therapeutic strategy to prevent for example age-related hearing loss. In a high-throughput screening the compound CLP257 and its carbamate prodrug derivate CLP290 were found as promising $KCC2$ agonist compounds that enhance the activity of $KCC2$ ^{93,94} and increase the phosphorylation of $Ser^{940/95}$. However, a follow-up study did not confirm the effect of CLP257 on $KCC2$ activity⁹⁶. Future studies should test whether this compound also has an influence on the phosphorylation of Ser^{937} .

In conclusion, we showed that a phospho-mimetic mutation of serine 937 enhances $KCC2$ activity in the mammalian auditory brainstem. This shifted the onset of hyperpolarisation, i.e. E_{Cl^-} , to an earlier timepoint in development and rendered E_{IPSC} in mature LSO and SPN neurons more negative. Thus, phospho-regulation of $KCC2$ is a potent way to increase its transport activity. As such, pharmaceuticals that directly interfere with phosphorylation of $KCC2$ may be a novel therapeutic strategy.

Material and methods

Construction of the expression clones

Site-directed mutagenesis of mouse $KCC2a$ (NM_001355480.1) was performed according to the QuikChange mutagenesis system (Stratagene, Heidelberg, Germany)^{65,66,97}. The sequence for the forward oligonucleotide for the generation of the $KCC2$ $Thr^{934Ala}/Ser^{937Asp}$ mutant is CGGGAGATCCAGAGCATCGCAGACGAGGACCGG GGTCCATTCCGGAG. The generated clone was verified by sequencing (LGC genomics, Berlin).

Cell culturing

For immunocytochemistry and measurement of K^+-Cl^- cotransporter activity, HEK293 cells were transiently transfected with the respective constructs, using Turbofect (Fermentas, Schwerte, Germany). Cells were seeded in a 6-well plate 24 h prior transfection. The DMEM medium was replaced four hours before transfection. 150 μ l Opti-MEM (Invitrogen, Karlsruhe, Germany), 6 μ l Turbofect and the corresponding DNA amount were thoroughly mixed and incubated for 20 min at room temperature. The mixture was applied to the cells which were then shaken at 300 rpm for 10 min at room temperature.

For K^+-Cl^- cotransporter activity measurements, transfected HEK293 cells were plated at a concentration of 1×10^5 cells/well in a 0.1 mg/ml poly-L-lysine coated black-well 96 well culture dish (Greiner Bio-One, Frickenhausen, Germany) 24 h after transfection. Each transfected construct was plated out three times, and represents three technical replicates. For the generation of independent biological replicates, the constructs were transfected separately. At least five biological replicates were done. The remaining cells were plated on 0.1 mg/ml poly-L-lysine-coated glass coverslips. After ~ 18 h, coverslips were proceeded for immunocytochemical analysis to determine transfection rates, which were routinely between 20 and 30%.

Immunocytochemistry

For immunocytochemistry, all steps were performed at room temperature. HEK293 cells grown on poly-L-lysine-coated coverslips were fixated for 10 min with 4% paraformaldehyde in 0.2 M phosphate buffer. Afterward, the cells were washed three times with PBS before the blocking solution (2% bovine serum albumin and 10% goat serum in PBS) was applied for 30 min. Primary antibody solution (anti-KCC2 N1-12; 1:1000; Neuromab, California, USA) was added in carrier solution (0.3% Triton X-100, 1% bovine serum albumin, 1% goat serum in PBS) and incubated for 1 h. After washing three times with PBS the secondary antibody, which was conjugated to a fluorescent probe (Alexa Flour 488 goat anti-mouse; 1:1000; Thermo Fisher Scientific, Bremen, Germany) was added to the carrier solution and incubated for 1 h. Again, the cells were washed three times with PBS and completely dried. The dried coverslips were mounted onto glass slides with Mowiol (Roth) and 4',6-diamidino-2-phenylindole (DAPI, 1:1000; Roth). Photomicrographs were taken using an Olympus fluorescence microscope (Olympus BX63).

Determination of the K⁺-Cl⁻ cotransport activity

Transport activity of KCC2 was determined by Cl⁻-dependent uptake of Tl⁺ in HEK293 cells as described previously^{72,73,98}. To initiate the flux measurement, the medium in the 96-well culture dish was replaced by 80 μ l hypotonic preincubation buffer (100 mM N-methyl-D-glucamine-chloride, 5 mM (4-(2-hydroxyethyl)-1-piperazineethanesulfonic acid) (Hepes), 5 mM KCl, 2 mM CaCl₂, 0.8 mM MgSO₄, 5 mM glucose, pH 7.4; osmolarity: 175 mmol/kg \pm 2) with 2 μ M FluoZin-2 AM dye (Invitrogen) plus 0.2% (wt/vol) Pluronic F-127 (Invitrogen) and incubated for 48 min at RT. Afterward, cells were washed three times with 80 μ l preincubation buffer and incubated for 15 min with 80 ml preincubation buffer including 0.1 mM ouabain to block the activity of the Na⁺/K⁺ ATPase. Then, the 96-well plate was placed into a fluorometer (Fluoroskan FL, Thermo Scientific), and each well was injected with 40 μ l 5 \times Thallium stimulation buffer (12 mM Tl₂SO₄, 100 mM N-methyl-D-glucamine 5 mM Hepes, 2 mM KCl, 2 mM CaCl₂, 0.8 mM MgSO₄, 5 mM glucose, pH 7.4). The fluorescence was measured in a kinetic-dependent manner (excitation 485 nm, emission 538 nm, one frame in 6 s in a 200-speriod) across the entire cell population in a single well. By using linear regression of the initial values of the slope of Tl⁺-stimulated fluorescence increase, the transport activity was calculated.

Statistical Analysis: Transport activities of the respective mutant were tested against control samples (*mm*KCC2a^{WT} and mock), using a two-sample *t*-test after Student's *t*-test for similar variances between samples. In exceptional cases, where the standard deviation differs by more than a factor of 2, Welch's *t*-test was used⁹⁹. To avoid pseudo-replication, the number of degrees of freedom was deflated according to the size of independent preparations each with three technical replicates. The false-discovery rate was controlled and *p*-values were corrected using the Benjamini–Hochberg method¹⁰⁰. The chance of false positive results (type I errors) was reduced by choosing *p*-values < 0.01.

The distribution of genotypes in the F1 generation was tested with the χ^2 test under the null hypothesis of a Mendelian ratio of 1:2:1. The age-dependent weight (P0–P16) was tested with repeated measurement two-way ANOVA against the null hypothesis of no difference in mean weight, using sex, genotype, and the interaction of sex and genotype as fixed factors and the mouse id as random factor, i.e., *aov(weight ~ sex*genotype + Error(id))*.

Animals

All protocols were in accordance with the German Animal Protection Law and approved by the local animal care and use committee (LAVES (Niedersächsisches Landesamt für Verbraucherschutz und Lebensmittelsicherheit), Oldenburg) and followed the NIH guide for the care and use of laboratory animals. Mice of both sexes were used. The KCC2^{AD/AD} mouse line was generated with CRISPR/Cas (clustered, regulatory interspaced, palindromic repeats (CRISPR)-associated (Cas) system) at the transgenic core facility at the Max Planck Institute of Molecular Cell Biology and Genetics (Dresden, Germany). For this purpose the guide RNA 5'cucguagugucgucacag 3' and the repair template: CATCCACTGTAGTAATGGCTCTTGGCAGGGCGTGGGTGGTGACCCCCAGCAGAGCTGGCACCAACCTGTGTCCTCCAGATCCAATCGATTGCCGATGAAGACCGAGGCTCCATT CGGAGGAA was used. These mice were kept on a C57Bl/6N genetic background. Primers for genotyping KCC2 wild-type are as follows: for: ATGGGCCCTTGAAGGACAGG and rev: CCGAGACTCGTCTGTGATGCT. For the genotyping of the T934A/S937D mutation in KCC2 the following primers were used: for: ATGGGCCCTTGAAGGACAGG, and rev: TCGGTCTTCATCGGCAATCGA.

Morphometric volume analysis

Adult KCC2^{AD/AD} and KCC2^{+/+} mice (aged between postnatal day (P) 30–P60) were transcardially perfused with phosphate buffered saline (PBS; 136.9 mM NaCl, 2.7 mM KCl, 10.1 mM Na₂HPO₄, 1.8 mM KH₂PO₄, pH 7.4) followed by 4% paraformaldehyde solution. Brains were dissected and postfixed for 2–4 h in 4% PFA and stored in 30% sucrose in PBS for cryoprotection. The brainstem was cut in coronal sections with a thickness of 30 μ m using a cryostat (Leica Biosystems, Wetzlar, Germany). Nissl staining was performed on consecutive sections of the auditory brainstem. Sections were imaged with an automated slide scanning microscope (AxioScan Z1, Carl Zeiss, Oberkochen, Germany). The volume of individual nuclei was obtained as described previously^{101–103}. Shortly, images were analysed by outlining the auditory nuclei using Fiji¹⁰⁴ and multiplying this area with the thickness of each section. Three animals per genotype were analysed. The experimentalist was blind to the respective genotype. Statistical analysis was performed using Student's *t*-test after testing for Gaussian distribution using Prism version 9 (GraphPad, San Diego, California). Reported values are mean \pm SD.

Patch-clamp recordings

Slice preparation: Coronal slices (200 μm) containing the superior olivary complex including LSO and SPN were cut from P3 to P29 mice of either sex. The brainstem was sliced with a vibratome (Leica VT1200 S), in ice-cold, low-calcium artificial cerebrospinal fluid (ACSF) solution containing (in mM): 125 NaCl, 2.5 KCl, 0.1 CaCl_2 , 3 MgCl_2 , 1.25 NaH_2PO_4 , 25 NaHCO_3 , 25 glucose, 2 sodium pyruvate, 3 myo-inositol, 0.5 ascorbic acid, continuously bubbled with 5% CO_2 and 95% O_2 , pH 7.4. Slicing solution contained lower Ca^{2+} and higher Mg^{2+} concentration than the standard ACSF in order to avoid Ca^{2+} -dependent signalling and activation of NMDAR. Slices were incubated in the standard recording solution (ACSF same as for slicing, except CaCl_2 and MgCl_2 were changed to 2 mM and 1 mM, respectively) for 30–45 min at 37 °C before being stored at room temperature until recordings.

Gramicidin perforated patch recordings were conducted at room temperature (22 ± 1 °C) in LSO neurons of P3 and P5 day old mice of both genotypes and either sex. Gramicidin perforated patch recordings were acquired as previously described^{77,78}. In brief, patch pipettes were pulled with DMZ-Universal-Electrode horizontal puller from filamented borosilicate glass capillaries (Science Products) to have resistances of 5–6 M Ω when filled with a K^+ -gluconate-based internal solution. Pipettes were tip-filled as follows (mM): 97.5 potassium-gluconate, 32.5 KCl, 1 MgCl_2 , 10 HEPES, 5 EGTA, 10 HEPES, pH 7.34 with KOH (290 mOsm). The remainder of the pipette was back-filled with the same solution including gramicidin (50 $\mu\text{g}/\text{ml}$ gramicidin A, Sigma) and 25 μM ATTO 488. The latter was used to confirm that the perforated patch was not ruptured. At the end of the experiment, the rupture of the perforated patch yielded E_{Cl^-} around the Nernst potential for Cl^- of -34 mV, thus confirming that the gramicidin ionophores were impermeable for Cl^- and that our recordings were not affected by the $[\text{Cl}^-]_{\text{pip}}$. The progress of perforation was evaluated by monitoring the steady-state current responses to a -5 mV voltage command (with access resistance dropping from 1 G Ω to around 20 M Ω). Recordings were done when series resistance reached a steady level (mean $R_s = 20.8 \pm 5$ M Ω , $n = 22$), typically within 30–40 min after the giga-seal formation. Glycine (1 mM) was prepared in standard recording ACSF and pressure applied (100 ms) over the soma of recorded neuron using a Picospritzer (General Valve Corp.). Current responses to glycine puff were recorded while cells were held at different holding potentials (from -82 to -12 mV with increment of 10 mV, offline corrected for liquid junction potential). The constant stimulation conditions were assured by controlling the pipette diameter, application pressure and duration, and distance from the cell (3 μm , 5 psi, 5 ms, 10 μm , respectively). The perfusion was turned off just prior to each puff application to avoid unequal dilution of the agonist. Significance of the responses was determined by employing the z -test, i.e., level of acceptance was set at $z < -3.3$ (I_m), which corresponds to $p < 0.001$ [$z = (A - \text{BL}) / \text{SD}_{\text{BL}}$, with A being the maximal amplitude of the response, BL the mean of the baseline (2 s prior to stimulation), SD_{BL} the standard deviation of the baseline]. Pressure-ejection of ACSF under the same condition evoked no response (mean ACSF response = -0.34 ± 0.2 pA, $z = -0.21 \pm 0.13$, $p > 0.73$, $n = 4$), while glycine evoked significant membrane currents in the same neurons.

Synaptic stimulation experiments were performed on LSO and SPN neurons of P14–P29 mice of both genotypes and either sex. Recordings were conducted at 37 ± 1 °C, maintained by an inline feedback temperature controller and heated stage (Warner Instruments) with the recording chamber being continuously perfused with ACSF at a rate of 1–2 ml min^{-1} . Whole-cell patch-clamp recordings were made from visually identified LSO and SPN neurons. Patch pipettes were pulled from borosilicate glass capillaries (Warner Instruments) using a DMZ Universal electrode puller (Zeitz-Instruments Vertriebs GmbH), filled with an internal solution containing (in mM): K-gluconate 97.5, KCl 32.5, HEPES 40, EGTA 5, MgCl_2 1, $\text{Na}_2\text{phosphocreatine}$ 5, pH was adjusted to 7.2 with KOH. Synaptic responses were evoked by afferent fibre stimulation with concentric bipolar electrodes (FHC inc., #CBARC75). Voltage pulses were generated by the HEKA amplifier and post-amplified by an isolated pulse stimulator (AM Systems). Inhibitory currents were recorded in ACSF containing 6,7-dinitroquinoline-2,3-dione (DNQX; 10 μM) and D-2-amino-5-phosphonopentanoic acid (D-AP5; 50 μM) to block AMPA and NMDA glutamate receptors, respectively. Stated voltages are corrected for a liquid junction potential of -11 mV.

The patch clamp recordings were acquired using a HEKA EPC 10 amplifier (HEKA Elektronik). Recorded signals were digitized at 50–100 kHz and filtered with a 6–10 kHz Bessel low-pass filter. Data were examined with FitMaster (HEKA) software followed by the analysis on the same software. Amplitude of the current responses from individual cells were plotted against holding potential under which they were recorded (IV diagram) and reversal potential was derived from linear fit of those values.

Statistics: Data sets were tested for Gaussian distribution prior to comparison with the Shapiro–Wilk test. Statistical analyses were carried out in Sigma Plot (Sigma Plot 14, Systat Software). Values are reported as mean \pm SEM and compared using t -test ($*p < 0.05$, $**p < 0.01$, $***p < 0.001$). The studies reported are in accordance with ARRIVE guidelines.

Data availability

All data generated or analysed during this study are included in this published article and its supplementary information files.

Received: 25 September 2023; Accepted: 30 November 2023

Published online: 08 December 2023

References

1. Turrigiano, G. G. & Nelson, S. B. Homeostatic plasticity in the developing nervous system. *Nat. Rev. Neurosci.* **5**, 97–107 (2004).
2. Eichler, S. A. & Meier, J. C. EI balance and human diseases—from molecules to networking. *Front. Mol. Neurosci.* **1**, 2 (2008).
3. Bormann, B. J., Hamill, O. P. & Sackmann, B. Mechanism of Anion permeation through channels gated by Glycine and γ -Aminobutyric acid in mouse cultured spinal neurones. *J. Physiol.* **385**, 243–286 (1987).

4. Cherubini, E., Rovira, C., Gaiarsa, J.-L., Corradetti, R. & Ben-Ari, Y. GABA mediated excitation in immature rat CA3 hippocampal neurons. *Int. J. Dev. Neurosci.* **8**, 481–490 (1990).
5. Cherubini, E., Gaiarsa, J.-L. & Ben-Ari, Y. GABA: an excitatory transmitter in early postnatal life. *Trends Neurosci.* **14**, 515–519 (1991).
6. Luhmann, H. J. & Prince, D. A. Postnatal maturation of the GABAergic system in rat neocortex. *J. Neurophysiol.* **65**, 247–263 (1991).
7. Zhang, B. L., Spigelman, I. & Carlen, P. L. Development of GABA-mediated, chloride dependent inhibition in CA1 pyramidal neurones of immature rat hippocampal slices. *J. Physiol.* **444**, 25–49 (1991).
8. Ehrlich, I., Löhrike, S. & Friauf, E. Shift from depolarizing to hyperpolarizing glycine action in rat auditory neurones is due to age-dependent Cl⁻ regulation. *J. Physiol.* **520**, 121–137 (1999).
9. Ben-Ari, Y., Gaiarsa, J.-L., Tyzio, R. & Khazipov, R. GABA: a pioneer transmitter that excites immature neurons and generates primitive oscillations. *Physiology* **87**, 1215–1284 (2007).
10. Yuste, R. & Katz, L. C. Control of postsynaptic Ca²⁺ influx in developing neocortex by excitatory and inhibitory neurotransmitters. *Neuron* **6**, 333–344 (1991).
11. Reichling, D. B., Kyrozis, A., Wang, J. & MacDermott, A. B. Mechanism of GABA and glycine depolarization-induced calcium transients in rat dorsal horn neurons. *J. Physiol.* **476**, 411–421 (1994).
12. Owens, D. F., Boyce, L. H., Davis, M. B. E. & Kriegstein, A. R. Excitatory GABA responses in embryonic and neonatal cortical slices demonstrated by gramicidin perforated-patch recordings and calcium imaging. *J. Neurosci.* **16**, 6416–6423 (1996).
13. Rohrbough, J. & Spitzer, N. C. Regulation of intracellular Cl⁻ levels by Na⁺-dependent Cl⁻-cotransport distinguishes depolarizing from hyperpolarizing GABA_A receptor-mediated responses in spinal neurons. *J. Neurosci.* **16**, 82–91 (1996).
14. Eilers, J., Plant, T. D., Marandi, N. & Konnerth, A. GABA-mediated Ca²⁺ signalling in developing rat cerebellar Purkinje neurones. *J. Physiol.* **536**, 429–437 (2001).
15. Kullmann, P. H., Ene, F. A. & Kandler, K. Glycinergic and GABAergic calcium responses in the developing lateral superior olive. *Eur. J. Neurosci.* **15**, 1093–1104 (2002).
16. Tozuka, Y., Fukuda, S., Namba, T., Seki, T. & Hisatsune, T. GABAergic excitation promoted neuronal differentiation in adult hippocampal progenitor cells. *Neuron* **47**, 803–815 (2005).
17. Redmond, L. & Ghosh, A. Regulation of dendritic development by calcium signaling. *Cell Calcium* **37**, 411–416 (2005).
18. Ben-Ari, Y., Cherubini, E., Corradetti, R. & Gaiarsa, J.-L. Giant synaptic potentials in immature rat CA3 hippocampal neurones. *J. Physiol.* **416**, 303–325 (1983).
19. Wu, W. L., Ziskind-Conhaim, L. & Sweet, M. A. early development of Glycine- and GABA-mediated synapses in rat spinal cord. *J. Neurosci.* **12**, 3935–3945 (1992).
20. Kandler, K. & Friauf, E. Development of Glycinergic and Glutamergic synaptic transmission on the auditory brainstem of perinatal rats. *J. Neurosci.* **15**, 6890–6904 (1995).
21. Blaesse, P., Airaksinen, M. S., Rivera, C. & Kaila, K. Cation-chloride cotransporters and neuronal function. *Cell* **61**, 820–838 (2009).
22. Kaila, K., Price, T. J., Payne, J. A., Puskarjov, M. & Voipio, J. Cation-chloride cotransporters in neuronal development, plasticity and disease. *Nat. Rev. Neurosci.* **15**, 637–654 (2014).
23. Delpire, E. Cation-Chloride Cotransporter in neuronal communication. *News Physiol. Sci.* **15**, 309–312 (2000).
24. Moore, Y. E., Kelley, M. R., Brandon, N. J., Deeb, T. Z. & Moss, S. J. Seizure control of KCC2: a new therapeutic target for epilepsy. *Trends Neurosci.* **40**, 555–571 (2017).
25. Payne, J. A., Rivera, C., Voipio, J. & Kaila, K. Cation-Chloride cotransporters in neuronal communication, development and trauma. *Trends Neurosci.* **26**, 199–206 (2003).
26. Virtanen, M. A., Uvarov, P., Mavrovic, M., Poncer, J. C. & Kaila, K. The multifaceted roles of KCC2 in cortical development. *Trends Neurosci.* **44**, 378–392 (2021).
27. Gamba, G. Molecular physiology and pathophysiology of electroneutral cation-chloride cotransporter. *Physiol. Rev.* **85**, 423–493 (2005).
28. Medina, I. *et al.* Current view on the functional regulation of the neuronal K⁺-Cl⁻ cotransporter KCC2. *Front. Cell. Neurosci.* **8**, 27 (2014).
29. Achilles, K. *et al.* Kinetic properties of Cl⁻ uptake mediated by Na⁺-dependent K⁺-2Cl⁻ cotransport in immature rat neocortical neurons. *J. Neurosci.* **27**, 8616–8627 (2007).
30. Ikeda, K. *et al.* Malfunction of respiratory-related neuronal activity in Na⁺, K⁺-ATPase L2 subunit-deficient mice is attributable to abnormal Cl⁻ homeostasis in brainstem neurons. *J. Neurosci.* **24**, 10693–10701 (2004).
31. Dzhalal, V. I. *et al.* NKCC1 transporter facilitates seizures in the developing brain. *Nat. Med.* **11**, 1205–1213 (2005).
32. Sung, K. W., Kirby, M., McDonald, M. P., Lovinger, D. & Delpire, E. Abnormal GABA_A receptor-mediated currents in dorsal root ganglion neurons isolated from Na-K-2Cl cotransporter null mice. *J. Neurosci.* **20**, 7531–7538 (2000).
33. Rivera, C. *et al.* The K⁺/Cl⁻ co-transporter KCC2 renders GABA hyperpolarizing during neuronal maturation. *Nature* **397**, 251–255 (1999).
34. Kaila, K. Ionic basis of GABA_A receptor channel function in the nervous system. *Prog. Neurobiol.* **42**, 489–537 (1994).
35. Hübner, C. A. *et al.* Disruption of KCC2 reveals an essential role of K-Cl cotransport already in early synaptic inhibition. *Neuron* **30**, 515–524 (2001).
36. Uvarov, P. *et al.* A novel N-terminal isoform of the neuron-specific K-Cl Cotransporter KCC2. *J. Biol. Chem.* **282**, 30570–30576 (2007).
37. Delpire, E., Lu, J., England, R., Dull, C. & Thorne, T. Deafness and imbalance associated with inactivation of the secretory Na-K-2Cl co-transporter. *Nat. Genet.* **22**, 192–195 (1999).
38. Delpire, E. & Mount, D. B. Human and murine phenotypes associated with defects in cation-chloride-cotransporter. *Annu. Rev. Physiol.* **64**, 803–843 (2002).
39. Zhu, L., Polley, N., Mathews, G. C. & Delpire, E. NKCC1 and KCC2 prevent hyperexcitability in the mouse hippocampus. *Epilepsy Res.* **79**, 201–212 (2008).
40. Clayton, G. H., Owens, D. F., Wolff, J. S. & Smith, R. L. Ontogeny of cation-Cl⁻ cotransporter expression in rat neocortex. *Dev. Brain Res.* **109**, 281–292 (1998).
41. Lu, J., Karadsheh, M. F. & Delpire, E. Developmental regulation of the neuronal-specific isoform of K-Cl cotransporter KCC2 in postnatal rat brains. *J. Neurobiol.* **39**, 558–568 (1999).
42. Gulyás, A. I., Sik, A., Payne, J. A., Kaila, K. & Freund, T. F. The KCl cotransporter, KCC2, is highly expressed in the vicinity of excitatory synapses in the rat hippocampus. *Eur. J. Neurosci.* **13**, 2005–2217 (2001).
43. Mikawa, S. *et al.* Developmental changes in KCC1, KCC2 and NKCC1 mRNAs in the rat cerebellum. *Dev. Brain Res.* **136**, 93–100 (2002).
44. Stein, V., Hermans-Borgmeyer, I., Jentsch, T. J. & Hübner, C. A. Expression of the KCl cotransporter KCC2 parallels neuronal maturation and the emergence of low intracellular chloride. *J. Comp. Neurol.* **468**, 57–64 (2004).
45. Yamada, J. *et al.* Cl⁻ uptake promoting depolarizing GABA actions in immature rat neocortical neurones is mediated by NKCC1. *J. Physiol.* **557**, 829–841 (2004).
46. Ge, S. *et al.* GABA regulates synaptic integration of newly generated neurons in the adult rat brain. *Nature* **439**, 589–593 (2006).

47. Balakrishnan, V. *et al.* Expression and function of chloride transporters during development of inhibitory neurotransmission in the auditory brainstem. *J. Neurosci.* **23**, 4134–4145 (2003).
48. Vale, C., Caminos, E., Martinez-Galan, J. R. & Juiz, J. M. Expression and developmental regulation of the K⁺-Cl⁻ cotransporter KCC2 in the cochlear nucleus. *Hear. Res.* **206**, 107–115 (2005).
49. Blaesse, P. *et al.* Oligomerization of KCC2 correlates with development of inhibitory neurotransmission. *J. Neurosci.* **26**, 10407–10419 (2006).
50. Hartmann, A.-M. *et al.* Opposite effect of membrane raft perturbation on transport activity of KCC2 and NKCC1. *J. Neurochem.* **111**, 321–331 (2009).
51. Kelsch, W. *et al.* Insulin-like growth factor 1 and a cytosolic tyrosine kinase activate chloride outward transport during maturation of hippocampal neurons. *J. Neurosci.* **21**, 8339–8347 (2001).
52. Rinehart, J. *et al.* Sites of regulated phosphorylation that control K-Cl cotransporter activity. *Cell* **138**, 525–536 (2009).
53. Kopp-Scheinflug, C. *et al.* The sound of silence: ionic mechanisms encoding sound termination. *Neuron* **71**, 911–925 (2011).
54. Yassin, L. *et al.* Nitric oxide signaling modulates synaptic inhibition in the superior paraolivary nucleus (SPN) via cGMP-dependent suppression of KCC2. *Front. Neural Circuits* **8**, 65 (2014).
55. Hartmann, A.-M. & Nothwang, H. G. NKCC1 and KCC2: Structural insights into phospho-regulation. *Front. Mol. Neurosci.* **15**, 964488 (2022).
56. Hartmann, A.-M. & Nothwang, H. G. Molecular and evolutionary insights into the structural organization of cation chloride cotransporters. *Front. Cell. Neurosci.* **8**, 470 (2015).
57. De los Heros, P. *et al.* The WNK-regulated SPAK/OSR1 kinases directly phosphorylate and inhibit the K⁺-Cl⁻ co-transporters. *Biochem. J.* **458**, 559–573 (2014).
58. Zhang, J. *et al.* Staurosporine and NEM mainly impair WNK-SPAK/OSR1 mediated phosphorylation of KCC2 and NKCC1. *PLOS ONE* **15**, e0232967 (2020).
59. Kahle, K. T. *et al.* Modulation of neuronal activity by phosphorylation of the K-Cl cotransporter KCC2. *Trends Neurosci.* **36**, 726–737 (2013).
60. Titz, S., Sammler, E. M. & Hormuzdi, S. G. Could tuning of the inhibitory tone involve graded changes in neuronal chloride transport? *Neuropharmacology* **95**, 321–331 (2015).
61. Markkanen, M. *et al.* Implications of the N-terminal heterogeneity for the neuronal K-Cl cotransporter KCC2 function. *Brain Res.* **1675**, 87–101 (2017).
62. Conway, L. C. *et al.* N-Ethylmaleimide increases KCC2 cotransporter activity by modulating transporter phosphorylation. *J. Biol. Chem.* **292**, 21253–21263 (2017).
63. Heubl, M. *et al.* GABA A receptor dependent synaptic inhibition rapidly tunes KCC2 activity via the Cl⁻-sensitive WNK1 kinase. *Nat. Commun.* **8**, 1–17 (2017).
64. Moore, Y. E., Deeb, T. Z., Chadchankar, H., Brandon, N. J. & Moss, S. J. Potentiating KCC2 activity is sufficient to limit the onset and severity of seizures. *Proc. Natl. Acad. Sci.* **115**, 10166–10171 (2018).
65. Weber, M., Hartmann, A.-M., Beyer, T., Ripperger, A. & Nothwang, H. G. A novel regulatory locus of phosphorylation in the C-terminus of the potassium chloride cotransporter KCC2 that interferes with N-ethylmaleimide or staurosporine mediated activation. *J. Biol. Chem.* **289**, 18668–18679 (2014).
66. Cordshagen, A., Busch, W., Winklhofer, M., Nothwang, H. G. & Hartmann, A.-M. Phosphoregulation of the intracellular termini of K⁺-Cl⁻ cotransporter 2 (KCC2) enables flexible control of its activity. *J. Biol. Chem.* **293**, 16984–16993 (2018).
67. Friedel, P. *et al.* WNK1-regulated inhibitory phosphorylation of the KCC2 cotransporter maintains the depolarizing action of GABA in immature neurons. *Science signaling* **8**, ra65 (2015).
68. Inoue, K. *et al.* Taurine inhibits K⁺-Cl⁻ cotransporter KCC2 to regulate embryonic Cl⁻ homeostasis via With-no-lysine (WNK) protein kinase signaling pathway. *J. Biol. Chem.* **287**, 20839–20850 (2012).
69. Lee, H. H. C. *et al.* Direct PKC-dependent phosphorylation regulates the cell surface stability and activity of the potassium chloride cotransporter, KCC2. *J. Biol. Chem.* **282**, 29777–29784 (2007).
70. Silayeva, L. *et al.* KCC2 activity is critical in limiting the onset and severity of status epilepticus. *Proc. Natl. Acad. Sci.* **112**, 3523–3528 (2015).
71. Hartmann, A.-M. & Nothwang, H. G. Molecular and evolutionary insights into the structural organization of cation chloride cotransporters. *Front. Cell. Neurosci.* **8**, 470 (2014).
72. Hartmann, A.-M., Fu, L., Ziegler, C., Winklhofer, M. & Nothwang, H. G. Structural changes in the extracellular loop 2 of the murine KCC2 potassium chloride cotransporter modulate ion transport. *J. Biol. Chem.* **296**, 100793 (2021).
73. Hartmann, A.-M., Pisella, L. I., Medina, I. & Nothwang, H. G. Molecular cloning and biochemical characterization of two cation chloride cotransporter subfamily members of *Hydra vulgaris*. *PLOS ONE* **12**, e0179968 (2017).
74. Kakazu, Y., Akaike, N., Komiyama, S. & Nabekura, J. Regulation of intracellular chloride by cotransporters in developing lateral superior olive neurons. *J. Neurosci.* **19**, 2843–2851 (1999).
75. Löhrke, S., Srinivasan, G., Oberhofer, M., Doncheva, E. & Friauf, E. Shift from depolarizing to hyperpolarizing glycine action occurs at different perinatal ages in superior olivary complex nuclei. *Eur. J. Neurosci.* **22**, 2708–2722 (2005).
76. Milenkovic, I. *et al.* Development of chloride-mediated inhibition in neurons of the anteroventral cochlear nucleus of gerbil (*Meriones unguiculatus*). *J. Neurophysiol.* **98**, 1634–1644 (2007).
77. Nerlich, J. *et al.* Dynamic fidelity control to the central auditory system: synergistic glycine/GABAergic inhibition in the cochlear nucleus. *J. Neurosci.* **34**, 11604–11620 (2014).
78. Witte, M. *et al.* Depolarizing chloride gradient in developing cochlear nucleus neurons: underlying mechanism and implication for calcium signaling. *Neuroscience* **261**, 207–222 (2014).
79. Akaike, N. Gramicidin perforated patch recording and intracellular chloride activity in excitable cells. *Prog. Biophys. Mol. Biol.* **65**, 251–264 (1996).
80. Kyrozis, A. & Reichling, D. B. Perforated-patch recording with gramicidin avoids artifactual changes in intracellular chloride concentration. *J. Neurosci. Methods* **57**, 27–35 (1995).
81. Sanes, D. H. & Friauf, E. Development and influence of inhibition in the lateral superior olivary nucleus. *Hear. Res.* **147**, 46–58 (2000).
82. Gillespie, D. C., Kim, G. & Kandler, K. Inhibitory synapses in the developing auditory system are glutamatergic. *Nat. Neurosci.* **8**, 332–338 (2005).
83. Alamilla, J. & Gillespie, D. C. Maturation of calcium-dependent GABA, glycine, and glutamate release in the glycinergic MNTB-LSO pathway. *PLOS ONE* **8**, e75688 (2013).
84. Milenkovic, I. & Rübsamen, R. Development of the chloride homeostasis in the auditory brainstem. *Physiol. Res.* **60**, S15 (2011).
85. Khirug, S. *et al.* Distinct properties of functional KCC2 expression in immature mouse hippocampal neurons in culture and in acute slices. *Eur. J. Neurosci.* **21**, 899–904 (2005).
86. Moore, Y. E. *et al.* Developmental regulation of KCC2 phosphorylation has long-term impacts on cognitive function. *Front. Mol. Neurosci.* **12**, 173 (2019).
87. Pisella, L. I. *et al.* Impaired regulation of KCC2 phosphorylation leads to neuronal network dysfunction and neurodevelopmental pathology. *Sci. Signal.* **12**, 0300 (2019).

88. Chamma, I., Chevy, Q., Poncer, J. C. & Lévi, S. Role of the neuronal K-Cl co-transporter KCC2 in inhibitory and excitatory neurotransmission. *Front. Cell. Neurosci.* **6**, 5 (2012).
89. Kullmann, P. H. & Kandler, K. Glycinergic/GABAergic synapses in the lateral superior olive are excitatory in neonatal C57Bl/6 mice. *Brain Res Dev Brain Res* **131**, 143–147. [https://doi.org/10.1016/s0165-3806\(01\)00271-1](https://doi.org/10.1016/s0165-3806(01)00271-1) (2001).
90. Noh, J., Seal, R. P., Garver, J. A., Edwards, R. H. & Kandler, K. Glutamate co-release at GABA/glycinergic synapses is crucial for the refinement of an inhibitory map. *Nat. Neurosci.* **13**, 232–238 (2010).
91. Lohrke, S., Srinivasan, G., Oberhofer, M., Doncheva, E. & Friauf, E. Shift from depolarizing to hyperpolarizing glycine action occurs at different perinatal ages in superior olivary complex nuclei. *Eur. J. Neurosci.* **22**, 2708–2722 (2005).
92. Rajaram, E., Pagella, S., Grothe, B. & Kopp-Scheinflug, C. Physiological and anatomical development of glycinergic inhibition in the mouse superior paraolivary nucleus following hearing onset. *J. Neurophysiol.* **124**, 471–483 (2020).
93. Gagnon, M. *et al.* Chloride extrusion enhancers as novel therapeutics for neurological diseases. *Nat. Med.* **19**, 1524–1528 (2013).
94. Puskarjov, M., Kahle, K. T., Ruusuvuori, E. & Kaila, K. Pharmacotherapeutic targeting of cation-chloride cotransporters in neonatal seizures. *Epilepsia* **55**, 806–818 (2014).
95. Barbour, A. J., Nass, S. R., Hahn, Y. K., Hauser, K. F. & Knapp, P. E. Restoration of KCC2 membrane localization in striatal dopamine D2 receptor-expressing medium spiny neurons rescues locomotor deficits in HIV Tat-transgenic mice. *ASN Neuro* **13**, 17590914211022088 (2021).
96. Cardarelli, R. A. *et al.* The small molecule CLP257 does not modify activity of the K⁺-Cl⁻ co-transporter KCC2 but does potentiate GABA A receptor activity. *Nat. Med.* **23**, 1394–1396 (2017).
97. Zhao, B. *et al.* A novel Di-leucine Motif mediated K⁺/Cl⁻ Cotransporter KCC2 internalization and is conserved amongst family members. *Cell. Signal.* **20**, 1769–1779 (2008).
98. Hartmann, A.-M. *et al.* Differences in the large extracellular loop between the K⁺-Cl⁻ cotransporters KCC2 and KCCA. *J. Biol. Chem.* **285**, 23994–24002 (2010).
99. Welch, B. L. J. B. The generalization of student's problem when several different population variances are involved. *Biometrika* **29**, 350–362 (1938).
100. Benjamini, Y. & Hochberg, Y. Controlling the false discovery rate: A practical and powerful approach to multiple testing. *J. R. Stat. Soc. Ser. B* **57**, 289–300 (1995).
101. Hirtz, J. J. *et al.* Cav1. 3 calcium channels are required for normal development of the auditory brainstem. *J. Neurosci.* **31**, 8280–8294 (2011).
102. Ebbers, L. *et al.* L-type calcium channel Cav1. 2 is required for maintenance of auditory brainstem nuclei. *J. Biol. Chem.* **290**, 23692–23710 (2015).
103. Krohs, C. *et al.* Loss of miR-183/96 alters synaptic strength via presynaptic and postsynaptic mechanisms at a central synapse. *J. Neurosci.* **41**, 6796–6811 (2021).
104. Schindelin, J. *et al.* Fiji: An open-source platform for biological-image analysis. *Nat. Methods* **9**, 676–682 (2012).

Acknowledgements

We thank the transgenic core facility at the Max Planck Institute of Molecular Cell Biology and Genetics (Dresden, Germany) for the generation of the transgenic mice. Authors are also grateful to Dr. Antje Cordshagen, Lauredana Alessandra Dos Santos Ferreira Grani, Natalie Ubben, and the animal facility at the University of Oldenburg. This work was supported by the Deutsche Forschungsgemeinschaft (Grants NO428/14-1 to H.G.N.; KO2207/3-1 to C.K.-S. and HA 6338/2-1 to A.-M.H.).

Author contributions

T.R., C.K.S., L.E., I.M., H.G.N. and A.M.H. designed the experiments, performed the experiments and analyzed the results. T.R., C.K.S. and M.W. performed statistical analyzes. A.M.H. wrote the paper with T.R., C.K.S., L.E., H.G., I.M., and M.W.

Funding

Open Access funding enabled and organized by Projekt DEAL.

Competing interests

The authors declare no competing interests.

Additional information

Supplementary Information The online version contains supplementary material available at <https://doi.org/10.1038/s41598-023-48884-x>.

Correspondence and requests for materials should be addressed to A.-M.H.

Reprints and permissions information is available at www.nature.com/reprints.

Publisher's note Springer Nature remains neutral with regard to jurisdictional claims in published maps and institutional affiliations.



Open Access This article is licensed under a Creative Commons Attribution 4.0 International License, which permits use, sharing, adaptation, distribution and reproduction in any medium or format, as long as you give appropriate credit to the original author(s) and the source, provide a link to the Creative Commons licence, and indicate if changes were made. The images or other third party material in this article are included in the article's Creative Commons licence, unless indicated otherwise in a credit line to the material. If material is not included in the article's Creative Commons licence and your intended use is not permitted by statutory regulation or exceeds the permitted use, you will need to obtain permission directly from the copyright holder. To view a copy of this licence, visit <http://creativecommons.org/licenses/by/4.0/>.

© The Author(s) 2023